Article

Conformationally Gated Switching between Superexchange and Hopping within Oligo-*p*-phenylene-Based Molecular Wires

Emily A. Weiss, Michael J. Tauber, Richard F. Kelley, Michael J. Ahrens, Mark A. Ratner, and Michael R. Wasielewski

J. Am. Chem. Soc., **2005**, 127 (33), 11842-11850• DOI: 10.1021/ja052901j • Publication Date (Web): 28 July 2005

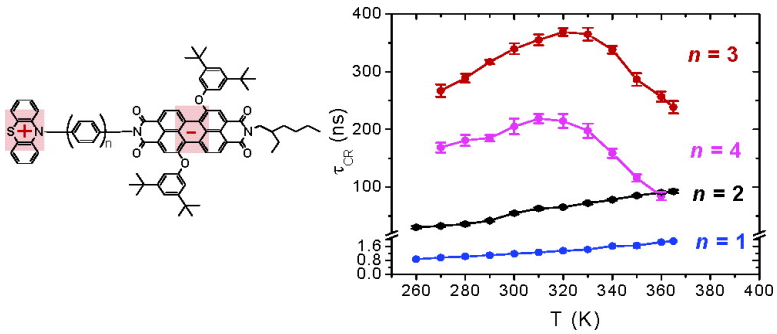

More About This Article

Additional resources and features associated with this article are available within the HTML version:

- Supporting Information
- Links to the 27 articles that cite this article, as of the time of this article download
- Access to high resolution figures
- Links to articles and content related to this article
- Copyright permission to reproduce figures and/or text from this article

View the Full Text HTML

J|A|C|S
ARTICLES
Published on Web 07/28/2005

Conformationally Gated Switching between Superexchange and Hopping within Oligo-*p*-phenylene-Based Molecular Wires

Emily A. Weiss, Michael J. Tauber, Richard F. Kelley, Michael J. Ahrens, Mark A. Ratner,* and Michael R. Wasielewski*

Contribution from the Center for Nanofabrication and Molecular Self-Assembly and Department of Chemistry, Northwestern University, Evanston, Illinois 60208-3113

Received May 3, 2005; E-mail: ratner@chem.northwestern.edu; wasielew@chem.northwestern.edu

Abstract: We observe well-defined regions of superexchange and thermally activated hopping in the temperature dependence of charge recombination (CR) in a series of donor−bridge−acceptor (D−B−A) systems, where D = phenothiazine (PTZ), B = *p*-phenylene (Ph_n), $n = 1-4$, and A = perylene-3,4:9,10-bis(dicarboximide) (PDI). A fit to the thermally activated CR rates of the $n = 3$ and $n = 4$ compounds yields activation barriers of 1290 and 2030 cm^{-1}, respectively, which match closely with theoretically predicted and experimentally observed barriers for the planarization of terphenyl and quaterphenyl. Negative activation of CR in the temperature regions dominated by superexchange charge transport is the result of a fast conformational equilibrium that increasingly depopulates the reactive state for CR as temperature is increased. The temperature dependence of the effective donor−acceptor superexchange coupling, V_{DA}, measured using magnetic field effects on the efficiency of the charge recombination process, shows that CR occurs out of the conformation with lower V_{DA} via the energetically favored triplet pathway.

Introduction

The transport of charge through molecules over lengths on the order of nanometers is necessary to bridge metal or semiconductor contacts within devices created with even the most sophisticated lithographic and epitaxial growth techniques. The portion of the transport that occurs solely on the molecule may be described by long-range electron transfer theories. The best model for efficient long-range electron transfer is the photosynthetic reaction center, within which tunneling and sequential mechanisms combine to move charge over nanometers with near unity quantum yield.[1−3]

There are three basic mechanisms available for molecular nonresonant charge-transfer processes. The first is superexchange,[4,5] where an electron or hole is transferred in a single step from donor to acceptor and the bridge is used as a medium for electronic coupling. In superexchange, the redox state of the bridge does not change, and the probability of transferring an electron/hole from donor to acceptor generally decreases exponentially with distance. The second mechanism is incoherent tunneling, where an electron or hole tunnels under successive energy barriers from one site to the next until it reaches a charge trap.[6−8] The temperature dependence of both of these mechanisms is very weak, arising from the electronic coupling between donor and acceptor (superexchange coupling) or between adjacent sites. The third mechanism is thermally activated hopping, where the energy barrier between sites is lowered enough by nuclear rearrangement that the system can be activated over the barrier.[6] The temperature dependence of the charge-transfer rate within this mechanism is fixed by the nuclear rearrangement, and the observed activation barrier should correspond to that of the relevant motion. Because the length dependence of incoherent charge-transfer mechanisms is weak, systems that utilize them are sometimes said to display molecular wire-like behavior.[9] Charge transfer within complex systems is due to some mixture of these three mechanisms,[10−12] with the proportion of each determined by energy matching of electronic levels and electronic coupling, which are in turn determined primarily by bridge length, conformational rigidity, temperature, and electronic properties of the redox centers.

We have previously observed molecular wire-like charge recombination in a series of donor−bridge−acceptor (D−B−A) systems, where the bridge is a *p*-phenylene (Ph_n) oligomer, $n = 1-5$.[13,14] The donor in these systems is phenothiazine (PTZ), and the acceptor is perylene-3,4:9,10-bis(dicarboximide)

(1) Deisenhofer, J.; Epp, O.; Miki, K.; Huber, R.; Michel, H. *J. Mol. Biol.* **1984**, *180*, 385.
(2) Fromme, P.; Kern, J.; Loll, B.; Biesiadka, J.; Saenger, W.; Witt, H. T.; Krauss, N.; Zouni, A. *Philos. Trans. R. Soc. London, B* **2002**, *357*, 1337.
(3) Witt, H. T. *Adv. Photosynth.* **1996**, *4*, 363.
(4) Bixon, M.; Jortner, J. *Adv. Chem. Phys.* **1999**, *106*, 35.
(5) Jortner, J.; Bixon, M.; Langenbacher, T.; Michel-Beyerle, M. E. *Proc. Natl. Acad. Sci. U.S.A.* **1998**, *95*, 12759.
(6) Berlin, Y. A.; Burin, A. L.; Ratner, M. A. *Chem. Phys.* **2002**, *275*, 61.
(7) Berlin, Y. A.; Burin, A. L.; Ratner, M. A. *J. Phys. Chem. A* **2000**, *104*, 443.
(8) Berlin, Y. A.; Hutchison, G. R.; Rempala, P.; Ratner, M. A.; Michl, J. *J. Phys. Chem. A* **2003**, *107*, 3970.
(9) Troisi, A.; Ratner, M. A.; Nitzan, A. *J. Chem. Phys.* **2003**, *118*, 6072.
(10) Segal, D.; Nitzan, A.; Davis, W. B.; Wasielewski, M. R.; Ratner, M. A. *J. Phys. Chem. B* **2000**, *104*, 3817.
(11) Segal, D.; Nitzan, A.; Ratner, M. A.; Davis, W. B. *J. Phys. Chem. B* **2000**, *104*, 2790.
(12) Paulson, B. P.; Miller, J. R.; Gan, W.-X.; Closs, G. L. *J. Am. Chem. Soc.* **2005**, *127*, 4860.
(13) Weiss, E. A.; Ahrens, M. J.; Sinks, L. E.; Ratner, M. A.; Wasielewski, M. R. *J. Am. Chem. Soc.* **2004**, *126*, 5577.
(14) Weiss, E. A.; Ahrens, M. J.; Sinks, L. E.; Ratner, M. A.; Wasielewski, M. A. *J. Am. Chem. Soc.* **2004**, *126*, 9510.

10.1021/ja052901j CCC: $30.25

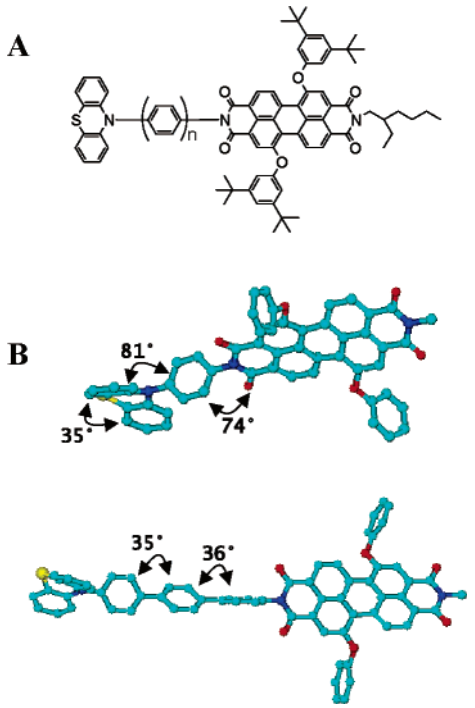

Figure 1. (A) Chemical structure of PTZ-Ph$_n$-PDI, where n = 1 for compound **1**, n = 2 for compound **2**, etc. (B) Representative DFT (B3LYP, 6-31G**) energy-minimized structures for **1** and **3** with their peripheral alkyl groups and hydrogen atoms not shown.

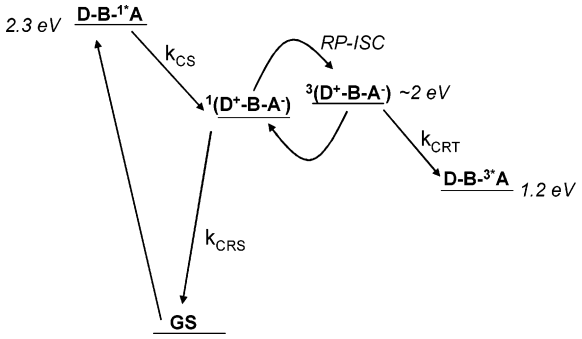

Figure 2. Charge-transfer scheme for **1**−**5**. Excitation at 400−420 or 532 nm gives the excited singlet state of the acceptor, A = PDI, followed by hole transfer to D = PTZ, resulting in the RP, ^{1}(D$^{+\bullet}$-B−A$^{-\bullet}$), B = Ph$_n$, which may undergo intersystem crossing to give ^{3}(D$^{+\bullet}$-B-A$^{-\bullet}$). Charge recombination may then occur from the singlet RP to the ground state, with rate k_{CRS}, or from the triplet RP to the locally excited triplet state, PTZ-Ph$_n$-^{3*}PDI, with rate k_{CRT}. The singlet−triplet splitting of the RP is given by the quantity 2J.

(PDI)[15] (Figure 1). Selective photoexcitation of PDI results in charge separation to produce a spin-coherent singlet radical ion pair (RP), ^{1}(PTZ$^{+\bullet}$-Ph$_n$-PDI$^{-\bullet}$), which subsequently undergoes radical pair intersystem crossing to yield ^{3}(PTZ$^{+\bullet}$-Ph$_n$-PDI$^{-\bullet}$). Spin-selective recombination from the RP singlet and triplet produces singlet ground state and excited triplet ^{3*}PDI, respectively (Figure 2 and Scheme 1). The energies of PTZ$^{+\bullet}$-Ph$_n^{-\bullet}$-PDI for n = 1−5 all are ≥3.0 eV above the respective ground states (and ≥1.0 eV above their respective PTZ$^{+\bullet}$-Ph$_n$-PDI$^{-\bullet}$ states), so that electron injection onto the bridge is very improbable, and charge recombination must proceed with an initial hole transfer onto the bridge. Calculations based on measured oxidation and reduction potentials of the molecular

Scheme 1. Orbital Occupancy Diagrams (frontier orbitals only) for Triplet (top) and Singlet Charge Recombination

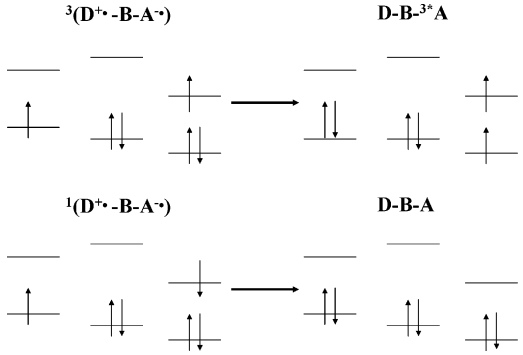

components[13,16,17] showed that, as the conjugation length of the bridge is increased, the energy of the charge-separated state in which the hole is localized on the bridge decreases. Additionally, through measurement of the electron spin−spin exchange interaction, 2J,[13,18,19] we unambiguously showed that the effective superexchange coupling, V_{DA}, decays exponentially with distance for n = 2−5. Thus, as observed experimentally, charge recombination is dominated by the superexchange mechanism for n = 1, 2, or 3 and by the incoherent hopping mechanism (PTZ$^{+\bullet}$-Ph$_n$-PDI$^{-\bullet}$ → PTZ-Ph$_n^{+\bullet}$-PDI$^{-\bullet}$ → PTZ-Ph$_n$-PDI) for n = 4 or 5 at room temperature.

In this paper, we explore the temperature dependence of the charge recombination mechanism within **1**−**4**. (The low charge separation yield in **5** prevented us from obtaining kinetic traces with sufficient signal-to-noise to yield accurate fits over a significant temperature range using transient absorption.) The dominant mechanism of charge transfer may be identified through the temperature dependence of the charge-transfer rate. Superexchange is the dominant mechanism in the shorter molecules (**1** and **2**) from 270 to 365 K and in the longer molecules (**3** and **4**) from 270 to ∼310 K. It is expected to dominate also at low temperatures, but we have not yet investigated this. The superexchange process is negatively activated in these systems because a fast conformational equilibrium depopulates the more reactive state for charge recombination as temperature is increased. We find that the switch in mechanism between superexchange and thermally activated hopping occurs at ∼310 K for **3** and **4**, and that this temperature dependence results from the dependence of bridge oxidation potential on conformational dynamics. It is well-known that the oxidized forms of poly-*p*-phenylene prefer a near-coplanar conformation, as the nuclear reorganization energy and the energy needed to overcome steric interactions are well compensated for by the ability of the charge to delocalize.[20,21] The switch in mechanism to incoherent hopping as a function of temperature in our systems is attributed to activation of bridge torsional motions above 310 K such that a majority of molecules contain oligo-*p*-phenylene bridges in the near-coplanar, easily oxidized conformation. The temperature at which this occurs depends on the activation barrier between the minimum-energy

(15) Van der Boom, T.; Hayes, R. T.; Zhao, Y.; Bushard, P. J.; Weiss, E. A.; Wasielewski, M. R. *J. Am. Chem. Soc.* **2002**, *124*, 9582.
(16) Meerholz, K.; Heinze, J. *Electrochim. Acta* **1996**, *41*, 1839.
(17) Marcus, R. A.; Sutin, N. *Biochim. Biophys. Acta* **1985**, *811*, 265.
(18) Lukas, A. S.; Bushard, P. J.; Weiss, E. A.; Wasielewski, M. R. *J. Am. Chem. Soc.* **2003**, *125*, 3921.
(19) Weiss, E. A.; Ratner, M. A.; Wasielewski, M. R. *J. Phys. Chem. A* **2003**, *107*, 3639.
(20) Szymoszek, A.; Koll, A. *Chem. Phys. Lett.* **2000**, *324*, 115.
(21) McCreery, R. L.; Anariba, F. *J. Phys. Chem. B* **2002**, *106*, 10355.

conformation and the easily oxidized conformation and the reduction potential of the bridge's redox partner, in this case, $PTZ^{+\bullet}$. Furthermore, in the incoherent hopping regime, the bridge torsional motion is rate-limiting, and activation barriers for hopping transport for **3** and **4** match well with known barriers for torsions within terphenyl and quaterphenyl oligomers.

Superexchange and Magnetic Field Effects

Superexchange[22−29] is the indirect exchange coupling of unpaired spins via filled orbitals which acquire paramagnetic character through mixing with charge-transfer excited-state configurations. Superexchange results in the virtual mediation of charge transfer from donor to acceptor via bridge orbitals that are energetically well-separated from those of the donor and acceptor. The superexchange coupling, V_{DA}, gives the effective interaction energy between the relevant orbitals on the donor and acceptor.[26−28] The donor−acceptor superexchange coupling, V_{DA}, in the paramagnetic RP state is the same coupling that determines the magnetic interaction between the unpaired spins of the RP. Therefore, the magnitude of the magnetic interaction, $2J$, and its behavior mirror that of V_{DA}. In fact, $2J$ is proportional to V_{DA}^2.[13,27,28,30−37]

The magnetic field effect (MFE) on the yield of ^{3*}PDI and the rate of RP recombination directly provides the magnitude of $2J$. The theory behind the MFE, including the mechanistic details of the radical pair intersystem crossing mechanism (RP−ISC), has been researched extensively[38−41] and applied to many donor−acceptor systems.[13,18,42−44] Following charge separation, the RP, initially formed in its singlet configuration, undergoes electron−nuclear hyperfine coupling-induced RP−ISC to produce the triplet RP. The subsequent charge recombination process is spin selective; that is, the singlet RP recombines to the singlet ground state, and the triplet RP recombines to yield the neutral local triplet PTZ-Ph_n-^{3*}PDI. Application of a static magnetic field splits the RP triplet levels, and variation of the field strength modulates the efficiency of the ISC by adjusting the energies of triplet RP sublevels relative to that of the singlet RP level. When the Zeeman splitting of the triplet RP levels equals the intrinsic singlet−triplet splitting, $2J$, of the RP, there is an increase in intersystem crossing rate. This increase translates into a maximum in triplet RP production and, therefore, a maximum in local triplet production upon recombination. By monitoring the yield of local triplet production as a function of applied magnetic field, $2J$—the magnitude of the magnetic superexchange interaction[27,45] —can be measured directly.

Experimental Section

Synthesis and Transient Absorption. The synthesis and characterization of compounds **1**−**4** have been reported previously.[13] A description of the femtosecond transient absorption apparatus can be found in the Supporting Information. The nanosecond transient absorption apparatus and the magnetic field effect experiment are described elsewhere.[13] For the variable temperature experiments, the sample temperature was maintained to within ±0.1 K by a thermostated cell holder (Quantum Northwest Flash 100). The sample was allowed to equilibrate for 30 min at each temperature prior to photolysis.

Results

Molecular Structure and Energy Levels. Figure 1 shows energy-minimized structures for **1** and **3**, which are representative of those for **1**−**4**. These structures and those of their corresponding radical ions (monocations or monoanions) were calculated in vacuum using density functional theory (unrestricted DFT for the open-shell systems) employing Becke's three-parameter hybrid functional using the Lee, Yang, and Parr correlation functional (B3LYP)[46,47] and a 6-31G** basis set with the Jaguar 5.3 software package.[48] The pucker angle of phenothiazine, calculated to be 147.70°, is in very good agreement with the value obtained from the X-ray structure, 146.11°.[49] PTZ and PDI are nearly perpendicular to their respective nearest-neighbor bridge units, and the twist angle between bridge units is ∼35°, which agrees well with angles obtained through other computational methods and basis sets.[50−52] In its cation state, PTZ is completely flat (a pucker angle of 180°) and is twisted 90° from an attached phenyl group. The geometry of the perylene core of PDI in its anion state is very similar to that in its neutral state; both have a significant twist angle between the naphthalenes in the perylene core. An attached phenyl is twisted ∼85° from PDI. Oligophenylene cation structures are flattened relative to their neutral geometries (Figure 3). The torsional angles between phenyl units are 20 and 23° in biphenyl cation and terphenyl cation, respectively. Within quaterphenyl cation, the inner two phenyl rings are twisted 23° with respect to each other and are twisted 27° with respect to the outer phenyl rings.

The effective distances between $PTZ^{+\bullet}$ and $PDI^{-\bullet}$ within $PTZ^{+\bullet}$-Ph_n-$PDI^{-\bullet}$, as well as those between $Ph_n^{+\bullet}$ and $PDI^{-\bullet}$ within PTZ-$Ph_n^{+\bullet}$-$PDI^{-\bullet}$ (Table S2), are measured from the

(22) Marcus, R. A. *Chem. Phys. Lett.* **1987**, *133*, 471.
(23) Ogrodnik, A.; Michel-Beyerle, M.-E. *Z. Naturforsch.* **1989**, *44a*, 763.
(24) Lukas, A. S.; Bushard, P. J.; Wasielewski, M. R. *J. Phys. Chem. A* **2002**, *106*, 2074.
(25) Kilsa, K.; Kajanus, J.; Macpherson, A. N.; Martensson, J.; Albisson, B. *J. Am. Chem. Soc.* **2001**, *123*, 3069.
(26) Kramers, H. A. *Physica* **1934**, *1*, 182.
(27) Anderson, P. W. *Phys. Rev.* **1959**, *115*, 2.
(28) Anderson, P. W. *Phys. Rev.* **1950**, *79*, 350.
(29) Weiss, E. A.; Sinks, L. E.; Lukas, A. S.; Chernick, E. T.; Wasielewski, M. R. *J. Phys. Chem. B* **2004**, *108*, 10309.
(30) Kobori, Y.; Sekiguchi, S.; Akiyama, K.; Tero-Kubota, S. *J. Phys. Chem. A* **1999**, *103*, 5416.
(31) Paddon-Row, M. N.; Shephard, M. J. *J. Phys. Chem. A* **2002**, *106*, 2935−2944.
(32) Volk, M.; Haberle, T.; Feick, R.; Ogrodnik, A.; Michel-Beyerle, M. E. *J. Phys. Chem.* **1993**, *97*, 9831.
(33) Closs, G. L.; Miller, J. R. *Science* **1988**, *240*, 440.
(34) Yamashita, J.; Kondo, J. *Phys. Rev.* **1958**, *109*, 730.
(35) Kramers, H. A. *Physica* **1934**, *1*.
(36) Closs, G. L.; Miller, J. R. *Science* **1988**, *240*, 440.
(37) Feher, G., Okamura, M., Eds. *Tunneling In Biological Systems*; Academic Press: New York, 1979.
(38) Weller, A.; Staerk, H.; Treichel, R. *Chem. Soc. Faraday Discuss.* **1984**, *78*, 271.
(39) Volk, M.; Haberle, T.; Feick, R.; Ogrodnik, A.; Michel-Beyerle, M.-E. *J. Phys. Chem.* **1993**, *97*, 9831.
(40) Till, U.; Hore, P. J. *Mol. Phys.* **1997**, *90*, 289.
(41) Steiner, U. E.; Ulrich, T. *Chem. Rev.* **1989**, *89*, 51.
(42) Tanimoto, Y.; Okada, N.; Itoh, M.; Iwai, K.; Sugioka, K.; Takemura, F.; Nakagaki, R.; Nagakura, S. *Chem. Phys. Lett.* **1987**, *136*, 42.
(43) Schulten, K.; Staerk, H.; Weller, A.; Werner, H.; Nickel, B. *Z. Phys. Chem. NF* **1976**, *101*, 371.
(44) Werner, U.; Kuhnle, W.; Staerk, H. *J. Phys. Chem.* **1993**, *97*, 9280.
(45) Shultz, D. A.; Fico, R. M.; Lee, H.; Kampf, J. W.; Kirschbaum, K.; Pinkerton, A. A.; Boyle, P. D. *J. Am. Chem. Soc.* **2003**, *125*, 15426.
(46) Lee, C.; Yang, W.; Parr, R. G. *Phys. Rev. B* **1988**, *37*, 785.
(47) Becke, A. D. *J. Chem. Phys.* **1993**, *98*, 1372.
(48) *Jaguar 3.5*; Schrodinger, Inc.: Portland, Oregon, 1998.
(49) Daub, J.; Engl, R.; Kurzawa, J.; Miller, S. E.; Schneider, S.; Stockmann, A.; Wasielewski, M. R. *J. Phys. Chem. A* **2001**, *105*, 5655.
(50) Heimel, G.; Daghofer, M.; Gierschner, J.; List, E. J. W.; Grimsdale, A. C.; Mullen, K.; Belijonne, D.; Bredas, J.-L.; Zojer, E. *J. Chem. Phys.* **2005**, *122*, 054501.
(51) Cacelli, I.; Prampolini, G. *J. Phys. Chem. A* **2003**, *107*, 8665.
(52) Honda, K.; Furukawa, Y. *J. Mol. Struct.* **2005**, *735*−*736*, 11.

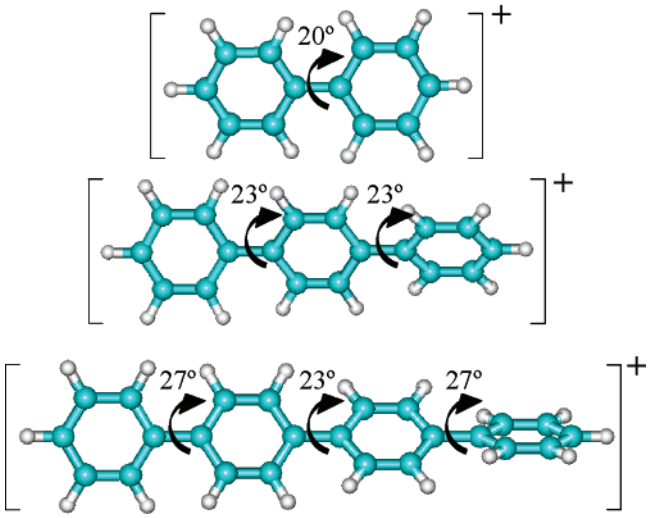

Figure 3. Unrestricted DFT (B3LYP, 6-31G**) energy-minimized structures of oligo-*p*-phenylene cations.

centroid of the unpaired spin distributions of $PDI^{-\bullet}$ relative to those of $PTZ^{+\bullet}$ and $Ph_n^{+\bullet}$, respectively. They range from 14 Å for $n = 1$ to 26 Å for $n = 4$. The spin distribution of each radical ion was obtained using the energy-minimized geometry of the radical ion at the UHF/AM1 level.[53] Energies of charge-separated states were estimated using Weller's expression based on the Born dielectric continuum model[54] of the solvent to determine the energy of formation of an ion pair in a solvent of arbitrary polarity.

Internal reorganization energies for charge recombination for **1**−**4** were obtained by performing single-point calculations (UHF) on the charged (cation for PTZ or Ph_n and anion for PDI) forms of the component molecules in the DFT-optimized ground state and ionic geometries and subtracting the SCF energy of the relaxed ionic configuration from that of the unrelaxed ground-state configuration.[8] Solvent reorganization energies for charge recombination were calculated from the Marcus formulation based on the dielectric continuum model of the solvent, where $\epsilon_S = 2.38$ and $\epsilon_\infty = 2.24$ for toluene.[17] Total reorganization energies are ∼0.6 eV for charge recombination in these systems and are listed in Table S3.

Absorption Spectra. The ground-state spectra of compounds **1**−**4**[13] have an absorption maximum at 550 nm ($\epsilon = 46\,000$ M^{-1} cm^{-1}), which is very similar to that of the PDI chromophore alone.[15] Additionally, there is a feature between 300 and 350 nm due to Ph_n that red-shifts and grows in intensity relative to the PDI bands as *n* increases. Spectroelectrochemical measurements show that the ground-state absorption spectrum of $PDI^{-\bullet}$ is characterized by a strong band peaked at 720 nm ($\epsilon = 79\,800$ M^{-1} cm^{-1}).[15] This feature is also present in the transient absorption spectrum spectra of **1**−**4** following photoexcitation of PDI with 400 nm, 130 fs laser pulses and 540 nm, 7 ns laser pulses (for **2**−**4**). The decay of this feature accompanies charge recombination in $PTZ^{+\bullet}$-Ph_n-$PDI^{-\bullet}$.

Temperature-Dependent Charge Recombination. Rate constants for recombination, k_{CR}, for **1**−**4** are plotted as a function of temperature in Figure 4. The recombination rate decreases monotonically with increasing temperature (CR is negatively activated) over the entire temperature range for **1** and **2** and from 270 to 320 K for **3** and **4**. The recombination rate within **3** and **4** then increases from 320 to 365 K.

Plots of ln k_{CR} versus $1/T$ for **3** and **4** in the positively activated region (320−365 K) are shown in Figure 5, while plots of $\ln(k_{CR} \times T^{1/2})$ versus $1/T$ for **1**−**4** in the negatively activated region are shown in Figure 6. The choice of rate laws used to describe these processes (and hence the choices of *y*-axes for these plots) will be explained in the Discussion. The data in the negatively activated region of **2** may be fit with a single line ($R^2 = 0.968$), but appears to fall into two distinct sections with barriers $E_a = -590 \pm 90$ cm^{-1} ($R^2 = 0.979$) and $E_a = -500 \pm 20$ cm^{-1} ($R^2 = 0.989$). The activation parameters (activation barriers, E_a, and prefactors, *A*) obtained from linear fits to the data in both regions are listed in Table 1.

Temperature-Dependent Magnetic Field Effects. Figure 7A shows a plot of ^{3*}PDI yield following RP recombination within **2** as a function of applied magnetic field for selected temperatures. The maximum of this plot, B_{2J}, is the field at which the RP−ISC process is most efficient because the singlet RP and one of the triplet RP sublevels have been brought into resonance, leading to increased production of ^{3*}PDI. This field, B_{2J}, corresponds to energy 2*J*, the splitting between the *S* and T_0 states of the RP. Figure 7B,C shows plots of the RP population, which is minimized at B_{2J}, for **3** (B) and **4** (C). The same values for 2*J* may be obtained from plots of ^{3*}PDI yield versus magnetic field for **3** and **4**, but the RP population plots have slightly better signal-to-noise over a larger temperature range. A MFE plot cannot be constructed for **1** because the RP does not live long enough to produce significant amounts of triplet recombination product via the magnetic field-sensitive radical pair mechanism.

Temperature-dependent magnetic field effect plots show the shift of 2*J* as a function of temperature due to the dependence of the effective coupling on the range of conformations sampled by the molecule.[55] The higher the field at which this resonance occurs, the greater the effective coupling between donor and acceptor. Figure 8 shows plots of ln 2*J* versus $1/T$ for **2**−**4** (with values listed in Table S4). Linear fits to the plots in Figure 8 yield activation barriers, $E_{a,2J}$, of 65 ± 34 cm^{-1} for **2** ($R^2 = 0.549$), 270 ± 20 cm^{-1} for **3** ($R^2 = 0.975$), and 300 ± 10 cm^{-1} for **4** ($R^2 = 0.990$), respectively. The distance decay parameter, α, where $2J = 2J_0 \exp(-\alpha r_{DA})$, has an average value of 0.34 $Å^{-1}$ and does not deviate more than 0.02 $Å^{-1}$ over the temperature range studied. We know of no other example of a direct measurement of the decay of the superexchange interaction through oligophenylene bridges, but our value for α may be compared to β values ($k_{eT} = k_0 \exp(-\beta r_{DA})$) obtained from distance-dependent rate measurements (α and β, though not exactly analogous, are both proportional to the square of an electronic coupling matrix element between donor and acceptor). Values for β from 0.32 to 0.66 $Å^{-1}$ have been measured for oligophenylene bridges.[13,56−62]

(53) *HyperChem*; Hypercube, Inc.; 1115 NW 4th Street, Gainesville, FL 32601, USA.
(54) Weller, A. *Z. Phys. Chem.* **1982**, *133*, 93.
(55) Weiss, E. A.; Tauber, M. J.; Ratner, M. A.; Wasielewski, M. R. *J. Am. Chem. Soc.* **2005**, *127*, 6052.
(56) Osuka, A.; Maruyama, K.; Mataga, N.; Asahi, T.; Yamazaki, I.; Tamai, N. *J. Am. Chem. Soc.* **1990**, *112*, 2.
(57) Helms, A.; Heiler, D.; McClendon, G. *J. Am. Chem. Soc.* **1992**, *114*, 6227.
(58) Kim, Y.; Lieber, C. M. *Inorg. Chem.* **1989**, *28*, 3990.
(59) Helms, A.; Heiler, D.; McClendon, G. *J. Am. Chem. Soc.* **1991**, *113*, 4325.

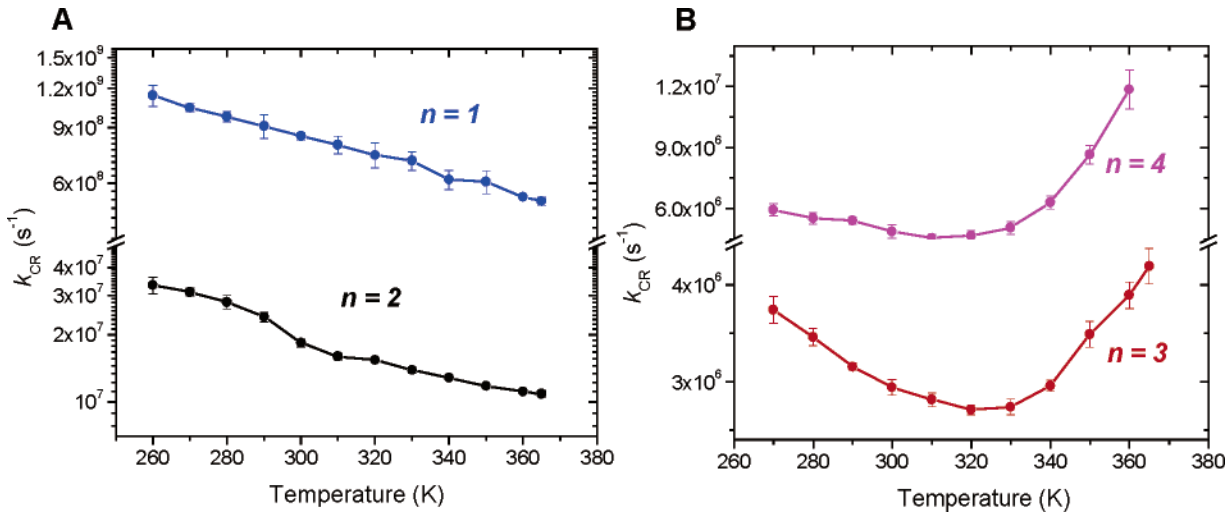

Figure 4. Plot of the rate constant for charge recombination, k_{CR}, versus temperature for **1** and **2** (A) and **3** and **4** (B).

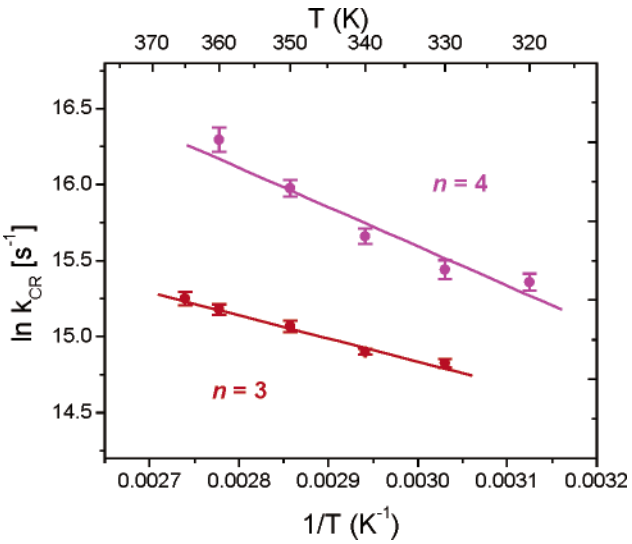

Figure 5. Plot of ln k_{CR} versus $1/T$ in the positively activated temperature regions for **3** (red) and **4** (magenta). Activation parameters are listed in Table 1.

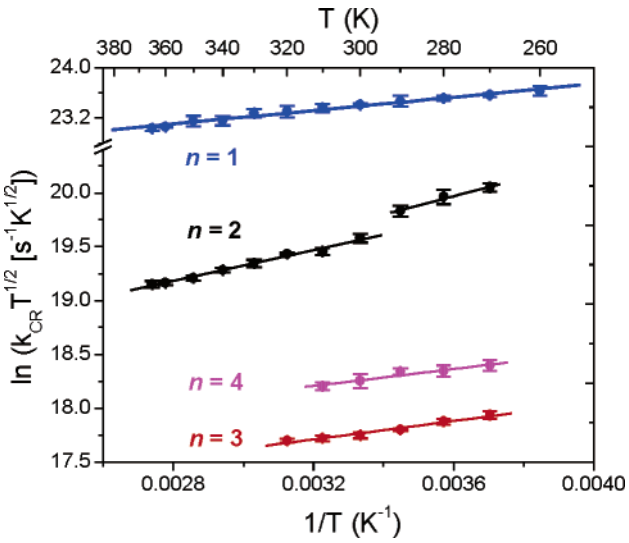

Figure 6. Plot of $\ln(k_{CR} \times T^{1/2})$ versus $1/T$ in the negatively activated temperature regions for **1** (blue), **2** (black), **3** (red), and **4** (magenta). Activation parameters are listed in Table 1.

Discussion

We have quantitatively determined the temperature-dependent behavior of the charge recombination rate for **1**−**4** and the superexchange coupling, $2J$, for **2**−**4** from 270 to 365 K. In the following discussion, we will first use room temperature magnetic field effects to determine the dominant pathway (singlet or triplet) for the charge recombination. We will then use activation barriers extracted from the temperature-dependent data to determine the mechanism of charge recombination over specific temperature regions. This analysis will allow us to clarify the nature of the switch in mechanism from superexchange to hopping and discuss the negative activation of superexchange charge recombination observed in these systems.

Table 1. Parameters for the Fit to the Temperature-Dependent Charge Recombination Rates of **1**−**4**, Plotted in Figures 5 and 6

compound	temperatures	model[a]	E_a	A	R^2
1	260−365 K	A	-370 ± 20 cm^{-1}	2.4×10^9 s^{-1}	0.989
2	270−290 K	A	-590 ± 90 cm^{-1}	2.2×10^7 s^{-1}	0.979
2	300−365 K	A	-500 ± 20 cm^{-1}	2.9×10^7 s^{-1}	0.989
3	270−320 K	A	-300 ± 20 cm^{-1}	1.3×10^7 s^{-1}	0.973
3	330−365 K	B	1060 ± 100 cm^{-1}	2.6×10^8 s^{-1}	0.985
4	270−310 K	A	-280 ± 40 cm^{-1}	2.3×10^7 s^{-1}	0.964
4	320−360 K	B	1910 ± 160 cm^{-1}	1.4×10^{10} s^{-1}	0.950

[a] Models A and B mean that the parameters were extracted from plots of $\ln(k_{CR} \times T^{1/2})$ versus $1/T$ and $\ln k_{CR}$ versus $1/T$, respectively.

Elucidation of the Dominant Recombination Pathway. Figure 9 shows plots of ^{3*}PDI yield (blue), RP population (red), and charge recombination rate (black) as a function of applied magnetic field for **3** at room temperature. The maximum of the triplet yield plot (and minimum of the RP yield plot) marks the field that corresponds to the energy, $2J$, the zero-field splitting of the singlet and triplet RP levels due to magnetic superexchange coupling. Figure 9 shows that $2J = 30$ mT for **3** at room temperature, and that at this field, the overall charge recombina-

(60) Osuka, A.; Satoshi, N.; Maruyama, K.; Mataga, N.; Asahi, T.; Yamazaki, I.; Nishimura, Y.; Onho, T.; Nozaki, K. *J. Am. Chem. Soc.* **1993**, *115*, 4577.
(61) Barigelletti, F.; Flamigni, L.; Balzani, V.; Collin, J.-P.; Sauvage, J.-P.; Sour, A.; Constable, E. C.; Cargill Thompson, A. M. W. *J. Am. Chem. Soc.* **1994**, *116*, 7692.
(62) Barigelletti, F.; Flamigni, L.; Guardgli, M.; Juris, A.; Beley, M.; Chodorowsky-Kimmes, S.; Collin, J.-P.; Sauvage, J.-P. *Inorg. Chem.* **1996**, *35*, 136.

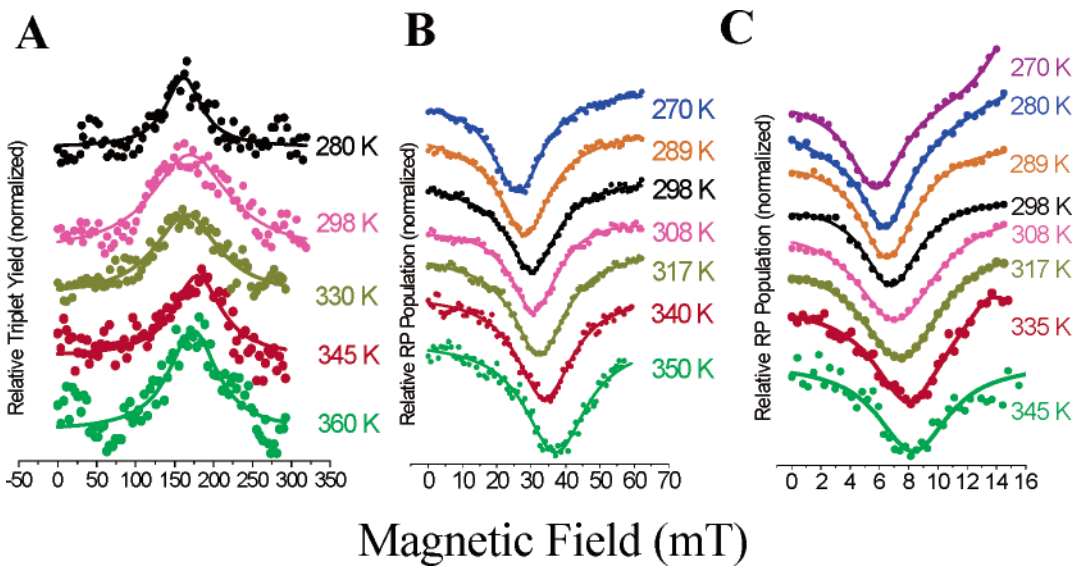

Figure 7. (A) Magnetic field effects on the population of the ^{3*}PDI monitored at 455 nm, produced upon recombination of the PTZ$^{+\bullet}$-Ph$_2$-PDI$^{-\bullet}$ RP, for selected temperatures; magnetic field effects on the population of the PTZ$^{+\bullet}$-Ph$_n$-PDI$^{-\bullet}$, $n = 3$ (B), $n = 4$ (C). RP monitored at 725 nm for selected temperatures. The lines through the scatter plots are Lorentzian (or multiple Lorentzian) fits with parameters given in Table S4.

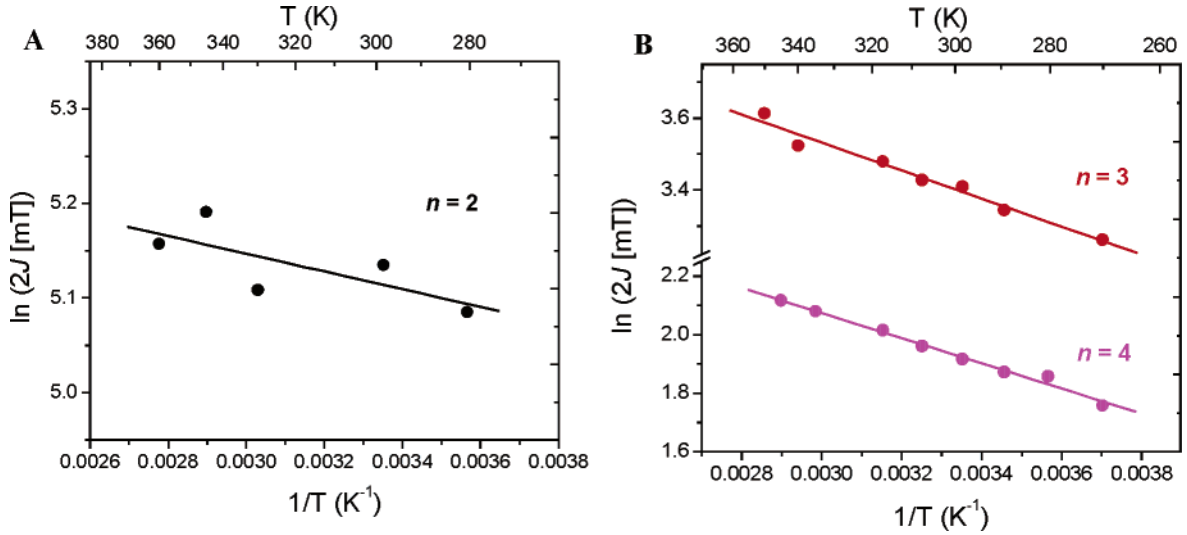

Figure 8. (A) Plot of ln(2J) versus 1/T and linear fit for **2** ($R^2 = 0.549$, $E_{a,2J} = 65 \pm 34$ cm^{-1}, $2J_0 = 230$ mT). (B) Plot of ln(2J) versus 1/T and linear fit for **3** ($R^2 = 0.975$, $E_{a,2J} = 270 \pm 20$ cm^{-1}, $2J_0 = 110$ mT) and **4** ($R^2 = 0.990$, $E_{a,2J} = 300 \pm 10$ cm^{-1}, $2J_0 = 29$ mT).

tion rate is maximized, implying that the triplet recombination pathway is significantly more efficient than the singlet pathway in **3**. This conclusion is reasonable considering that the energy gap for singlet recombination ($-\Delta G_{CRS}$) is 2.1 eV for **3** and, therefore, lies deep in the so-called Marcus-inverted region of the rate versus free energy of reaction profile (where $\lambda = 0.6$ eV).[63] The energy gap for triplet recombination ($-\Delta G_{CRT}$) is 0.9 eV for **3** and, therefore, lies near the top of the Marcus curve. The corresponding plot for **4** ($2J = 6.8$ mT) is similar to that in Figure 9. The recombination rate is not sensitive to magnetic field strength in **2**, so there is no competition between singlet and triplet pathways. Since significant ^{3*}PDI is produced in **2**, this implies that the triplet pathway is used almost exclusively.

Thermally Activated Transport. In previous work on these systems at room temperature,[13] we observed that the charge recombination rate decreased exponentially with bridge length for $n = 1-3$, after which it increased slowly from $n = 3-5$. We concluded that the switch from superexchange-dominated transport to hopping-dominated transport occurs at $n = 3$. It can be seen from Figures 4 and 6 that compounds **3** and **4** show clearly defined regions of positive activation above ~310 K, similar to the point at which McCreery and co-workers[21] saw the onset of activated behavior within a terphenyl monolayer junction. Thus, the temperature dependence indicates that the terphenyl bridge is the smallest basic unit in which the intermediate PTZ-Ph$_n^{+\bullet}$-PDI$^{-\bullet}$ state is accessed.

The positive activation of the CR rate in **3** and **4** implies that the hopping process is enabled by the molecular motions of the bridge. In the neutral ground state, experiment and theory agree that the torsional angles within oligo-*p*-phenylene are between 35 and 40° (Figure 1),[20,50−52,64,65] while oxidized oligophenylenes prefer a more coplanar, quinoid-type geometry (Figure 3).[66,67] Phenyl ring dynamics are governed by the

(63) Marcus, R. A. *J. Chem. Phys.* **1965**, *43*, 679.

(64) Goller, A.; Grummt, U.-W. *Chem. Phys. Lett.* **2000**, *321*, 399.

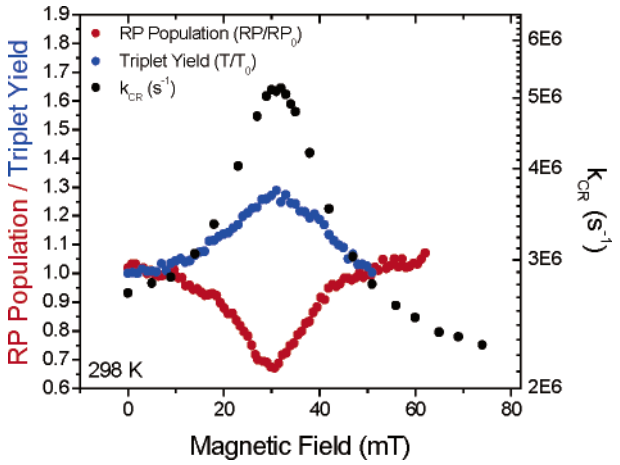

Figure 9. Magnetic field effects on the rate of PTZ^{+}-Ph_3-PDI^{-} RP recombination (black), the population of the RP (red), and triplet yield (blue) at 298 K. The recombination rate is maximized at 2*J*, where triplet yield is maximized and RP population is minimized, indicating that the triplet recombination pathway is more efficient than the singlet pathway.

competition between the benefit of the conjugation gained by a coplanar geometry and the cost of steric repulsion between the ortho hydrogens of the phenyl rings.[52,68,69] The importance of strong anharmonic torsional modes in the dynamics of oligo-*p*-phenylene is well-accepted, and inclusion of the double-well torsional potential for shorter oligomers is necessary in modeling ground-state electronic properties.[20,50−52]

Figure 10 shows the total energies of electronic states relevant to the first step of incoherent hopping charge recombination, a hole transfer from PTZ cation to the bridge: $PTZ^{+\bullet}$-Ph_n-$PDI^{-\bullet}$ → PTZ-$Ph_n^{+\bullet}$-$PDI^{-\bullet}$. The energy levels of PTZ-$Ph_n^{+\bullet}$-$PDI^{-\bullet}$ states are calculated for two different bridge geometries, a neutral geometry (like those in Figure 1) and an optimized cation geometry (like those in Figure 3). The energies of the states in the neutral bridge geometries are calculated as described previously[70] with the Weller equation,[54] in which measured electrochemical potentials of the bridge and PDI are combined with Coulomb and solvent dielectric stabilization terms to get an estimate of the free energy of the ion pair relative to the neutral ground state. Those for cation geometries are obtained using the same equation, except that the measured oxidation potential of the bridge is adjusted by a calculated (DFT, B3LYP, 6-31G*) energy ΔE_{HOMO}. ΔE_{HOMO} is the difference between the energy of the filled bridge HOMO when the bridge is in an optimized neutral geometry and the energy of the filled bridge HOMO when the bridge is in an optimized cation geometry. As the temperature is increased and bridge torsional modes are activated, there is increasing population in the more coplanar geometries, and charge-transfer reaction $PTZ^{+\bullet}$-Ph_n-$PDI^{-\bullet}$ → PTZ-$Ph_n^{+\bullet}$-$PDI^{-\bullet}$ becomes more probable. One can clearly see from this figure that, even if the temperature were high enough for the biphenyl bridge to spend a significant amount of time in the optimal cation configuration, the hole transfer to the bridge is still ∼0.5 eV uphill. Therefore, charge recombination within **2** (and, by the same reasoning, in **1**) avoids actual hole transfer to the bridge and instead proceeds primarily through superexchange from 270 to 365 K. However, activation of torsional modes in terphenyl and quaterphenyl will allow a significant population of molecules to sample conformations where the bridge can be oxidized. The temperature-dependent data obtained here indicate that this behavior is found in **3** and **4** at $T > 310$ K.

The hopping mechanism may be thought of as an equilibrium process between a conformational state in which the bridge cannot be oxidized and a state in which it may be oxidized, followed by a hole transfer onto the bridge:

$$PTZ^{+\bullet}\text{-}Ph_n\text{-}PDI^{-\bullet}(conf\ 1) \underset{k_{-1}}{\overset{k_1}{\rightleftharpoons}} PTZ^{+\bullet}\text{-}Ph_n\text{-}PDI^{-\bullet}(conf\ 2) \xrightarrow{k_2} PTZ\text{-}Ph_n^{+\bullet}\text{-}PDI^{-\bullet} \quad (1)$$

where *conf 1* is the minimum energy bridge conformation and *conf 2* is the near-coplanar bridge conformation. The steady-state solution for the observed rate of formation of PTZ-$Ph_n^{+\bullet}$-$PDI^{-\bullet}$ is[71−76]

$$k_{obs} = \frac{k_1 k_2}{k_{-1} + k_2} \quad (2)$$

The hole transfer process, k_2, is very fast once its barrier is lowered by the activated torsional motion, so $k_2 \gg k_{-1}$ and $k_{obs} = k_1$. The temperature dependence of the slow torsional motion (and therefore the observed rate) is governed by the transition state theory expression[77]

$$k_{obs} = A_1 \exp(-E_{a,1}/k_B T) \quad (3)$$

A fit of the rate data for **3** and **4** within the positively activated region to eq 3 (Figure 5) yields barriers, $E_{a,1}$, of 1060 ± 100 cm^{-1} ($A_1 = 2.6 \times 10^8$ s^{-1}) for **3** and 1910 ± 160 cm^{-1} ($A_1 = 1.4 \times 10^{10}$ s^{-1}) for **4**.[78] These numbers are very similar to DFT-calculated (B3LYP, triple-ζ polarized basis set) barriers of 1330 and 1910 cm^{-1} for the planarization of terphenyl and quaterphenyl, respectively,[51,79,80] and to the 1530 cm^{-1} barrier for the planarization of terphenyl obtained from a corrected Hartree−Fock (6-311G(d,p)) potential.[50] Estimated barrier heights for internal ring rotation within terphenyl in solution hover around 1600 cm^{-1};[52,81,82] similar studies are not available for quaterphenyl. Through carbon-13 NMR relaxation data (in chloroform), Tekely et al.[83] estimated the activation barrier for the

(65) Grein, F. *Theor. Chem. Acc.* **2003**, *109*, 274.
(66) Moliton, A.; Hiorns, R. C. *Polym. Int.* **2004**, *53*, 1397.
(67) Bredas, J.-L.; Chance, B.; Silbey, R. *Phys. Rev. B* **1982**, *26*, 5843.
(68) Tsuzuki, S.; Uchimaru, T.; Matsumura, K.; Mikami, M.; Tanabe, K. *J. Chem. Phys.* **1999**, *110*, 2858.
(69) Pan, J.-F.; Chua, S.-J.; Huang, W. *Thin Solid Films* **2000**, *363*, 1.
(70) Weiss, E. A.; Ahrens, M. J.; Sinks, L. E.; Gusev, A. V.; Ratner, M. A.; Wasielewski, M. R. *J. Am. Chem. Soc.* **2004**, *126*, 5577.
(71) Davis, W. B.; Ratner, M. A.; Wasielewski, M. R. *J. Am. Chem. Soc.* **2001**, *123*, 7877.
(72) Kiselev, V. D.; Miller, J. R. *J. Am. Chem. Soc.* **1975**, *97*, 4036.
(73) Zaman, K. M.; Yamamoto, S.; Nishimura, N. *J. Am. Chem. Soc.* **1994**, *116*, 12099.
(74) Yamamoto, S.; Sakurai, T.; Yingjin, L.; Sueishi, Y. *Phys. Chem. Chem. Phys.* **1999**, *1*, 833.
(75) Fukuzumi, S.; Ohkubo, K.; Tokuda, Y.; Suenobu, T. *J. Am. Chem. Soc.* **2000**, *122*, 4286.
(76) Frank, R.; Greiner, G.; Rau, H. *Phys. Chem. Chem. Phys.* **1999**, *1*, 3841.
(77) Steinfeld, J. I.; Francisco, J. S.; Hase, W. L. *Chemical Kinetics and Dynamics*, 2nd ed.; Prentice Hall, Inc.: Upper Saddle River, NJ, 1999.
(78) Berlin, Y. A.; Burin, A. L.; Ratner, M. A. *Chem. Phys.* **2002**, *275*, 61.
(79) Blankenship, R. E. *Acc. Chem. Res.* **1981**, *14*, 163.
(80) DFT is considered a reliable technique for studying energy barriers and conjugation in oligophenylenes, and DFT calculations with a moderate basis set agree with MP2 calculations using an extensive cc-pVQZ basis set for biphenyl.
(81) Tkaczyk, S. W. *Proc. SPIE-Int. Soc. Opt. Eng.* **2001**, *4413*, 226.
(82) Melzer, P.; Kurreck, H.; Kieslich, W. *Chem. Ber.* **1982**, *115*, 3597.
(83) Tekely, P.; Laupretre, F.; Monnerie, L. *Macromolecules* **1983**, *16*, 415.

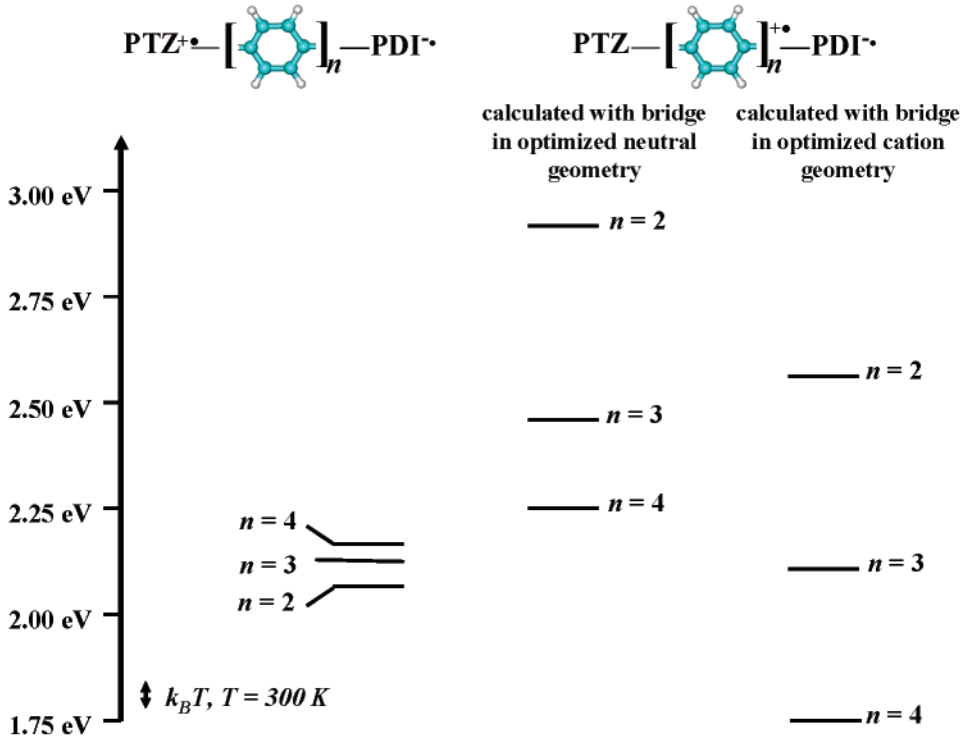

Figure 10. Energy level diagram for states relevant to the initial step of incoherent CR: $PTZ^{+\bullet}$-Ph_n-$PDI^{-\bullet}$ → PTZ-$Ph_n^{+\bullet}$-$PDI^{-\bullet}$.

rotation of the external phenyl rings within *p*-terphenyl to be 1230 cm^{-1}. We may confidently conclude that the torsional motions of the terphenyl and quaterphenyl bridges within **3** and **4** are gating the initial, rate-determining step of the charge recombination (the fast oxidation of the bridge) within **3** and **4** in the positively activated region.

As detailed in the Supporting Information, we also attempted to fit the rate data for **3** and **4** in the positively activated region to semiclassical Marcus theory, but this theory predicts a significantly higher barrier for charge recombination in **3** than in **4**, which is clearly not observed here.

Superexchange Transport. Below 310−320 K in **3** and **4** and for all temperatures in **2**, the torsional motions of the bridge are insufficiently activated to permit the majority of molecules to recombine via hopping, and the weak temperature dependence of k_{CR} indicates that superexchange dominates. However, rather than a temperature-independent recombination rate, we observe a decreased rate of charge recombination with increased temperature in the superexchange region for **1**−**4**.

The negative activation of observed CR rate can be explained with a pre-equilibrium mechanism in which increased temperature leads to conformational dynamics that deplete the state favorable for electron transfer.[55,72−76] In this case, the set of motions that cause the depletion of the reactive state are most likely a combination of low-barrier torsions and vibrations of the bridge, donor, and acceptor. These dynamics may be represented by a fast equilibrium process between RP states such that the total superexchange process is

$$PTZ^{+\bullet}\text{-}Ph_n\text{-}PDI^{-\bullet}(conf\ 1') \underset{k_{-1}'}{\overset{k_1'}{\rightleftharpoons}} PTZ^{+\bullet}\text{-}Ph_n\text{-}PDI^{-\bullet}\ (conf\ 2') \xrightarrow{k_2'} PTZ\text{-}Ph_n\text{-}^{3*}PDI \quad (4)$$

Here, *conf 2′* is the more reactive conformer. The steady-state solution for the formation of product within the scheme of eq 4 is again given by eq 2. The fact that this process is primarily a tunneling event implies that the actual electron-transfer step, k_2', is very slow relative to the conformational dynamics. Therefore, $k_{-1}' \gg k_2'$, and eq 2 reduces to

$$k_{obs} = K_{eq}k_2' = \exp(-\Delta G_{12}/k_BT) \times A_2 \exp(-E_{a,2}/k_BT) \quad (5)$$

where $E_{a,2}$ is the activation energy for the elementary charge-transfer reaction. ΔG_{12}, the free energy difference between *conf 1′* and *conf 2′*, must be negative if *conf 2′* is increasingly depleted at higher temperatures. The observed barrier for CR, $E_{a,obs}$, is $(\Delta G_{12} + E_{a,2})$. For ΔG_{12} negative and $|\Delta G_{12}| > E_{a,2}$, $E_{a,obs}$ will be negative, and k_{obs} will decrease as temperature increases.

Since $PTZ^{+\bullet}$-Ph_n-$PDI^{-\bullet}$ (*conf 2′*) → PTZ-Ph_n-^{3*}PDI is an elementary nonadiabatic charge-transfer reaction, its rate should be adequately described by a semiclassical treatment, $k_2' = (2\pi/h)V_{CR}^2$FCWD, where FCWD is the Franck−Condon weighted density of states. In this treatment, $A_2 \propto 1/T^{1/2}$. A plot of ln $k_{obs} \times T^{1/2}$ versus $1/T$ (Figure 6) will have slope of $-(\Delta G_{12} + E_{a,2})$. There are then two reasons why *conf 2′* may be the preferred reactant state for charge recombination: better electronic coupling or better vibronic overlap[84−88] with the product state, PTZ-Ph_n-^{3*}PDI. Over the temperature range within which charge recombination is negatively activated in **2**−**4**, $2J$, which is proportional to V_{DA}^2, increases, indicating that the effective donor−acceptor coupling increases with temperature (Figure 7). Therefore, *conf 1′*, the state that is increasingly populated at

(84) Scherer, P. O. J.; Fischer, F. *Chem. Phys. Lett.* **1987**, *141*, 179.
(85) Vauthey, E.; Suppan, P. *Chem. Phys.* **1989**, *139*, 381.
(86) Woodbury, N. W.; Becker, M.; Middendorf, D.; Parson, W. W. *Biochemistry* **1985**, *24*, 7516.
(87) Bixon, M.; Jortner, J. *J. Phys. Chem.* **1991**, *95*, 1941.
(88) Buhks, E.; Jortner, J. *FEBS Lett.* **1980**, *109*, 117.

higher temperature, is the state with higher electronic coupling. Interestingly, the preferred reactant state for CR is the lower-coupling state, *conf 2′*.

It is then likely that the temperature dependence of the Franck−Condon factor is responsible for negative activation of charge recombination. In the classical limit, the temperature dependence of the FCWD is dominated by the barrier

$$\exp[(-\Delta G_{CR} + \lambda)^2/4\lambda k_B T] \quad (6)$$

The total reorganization energy, $\lambda = \sim 0.6$, for **1**−**4** and the values for ΔG_{CR} range from approximately −0.7 eV for **1** to −1.0 eV for **4**. The value for λ may be underestimated because a dielectric continuum model is widely considered to be an inadequate description of the reorganization of nondipolar moments in toluene.[89] Because $-\Delta G_{CR} \approx \lambda$, the potential surface of the product, PTZ-Ph$_n$-^{3*}PDI, intersects that of the reactant, PTZ$^{+\bullet}$-Ph$_n$-PDI$^{-\bullet}$, near its minimum. Therefore, the $v = 0$ vibrational state of the reactant overlaps best with the product surface. It is possible that, as the temperature is increased, higher-lying, less-reactive vibrational states are populated, and the rate of charge recombination decreases. Negative activation of exergonic electron transfer in a variety of systems has been attributed to this mechanism.[84−88,90]

Effect of the Conformational Equilibrium on the Temperature Dependence of 2*J*. Electronic coupling is not the cause of negative activation in these systems; nonetheless, an interesting result may be obtained from the temperature dependence of 2*J*. The data for **3** and **4**, when plotted as ln 2*J* versus 1/*T*, fit well to a linear regression with a slope of −270 ± 20 cm^{-1} for **3** and −300 ± 10 cm^{-1} for **4** (Figure 8). The temperature dependence of the effective 2*J* fits a transition-state theory form because it is an average singlet−triplet splitting for RPs in multiple conformations that exchange rapidly on the time scale of the magnetic field effect experiment. The temperature dependence derives from that of the equilibrium constant between the relevant conformations.[55]

The barriers extracted from the plots of ln 2*J* versus 1/*T* are the same not only within experimental error ($\Delta G_{12} \cong 290$ cm^{-1}) but also the same magnitude (with opposite sign) as the slopes of the rate plots for **3** and **4** in the negatively activated regions, $(\Delta G_{12} + E_{a,2}) \sim -280$ cm^{-1}. The pre-equilibrium model relies on the fact that the k_{-1}' process is much more sensitive to temperature than the k_2' process, such that *conf 2′* is increasingly depleted by k_{-1}' as the temperature is increased and the observed rate of recombination slows. Therefore, $E_{a,2} \ll |\Delta G_{12}|$ and $(\Delta G_{12} + E_{a,2}) \approx \Delta G_{12} = -280$ cm^{-1}, which matches the value obtained from the 2*J* plot. So, when the charge recombination proceeds by the mechanism in eq 4, we may obtain the free energy difference between conformational states of the molecule via two different methods, the temperature dependence of the rate, and the temperature dependence of 2*J*.

The actual values of the barriers obtained from the plots in Figures 6 and 8 cannot be assigned unambiguously to specific molecular motions without systematic molecular dynamics simulations and electronic structure calculations. Because there is a significant geometry change upon the conversion of PTZ from its cation state to its neutral state,[91] we suspect that the relevant motions are those vibrations and rotations centered around the linkage between the phenothiazine nitrogen and the adjacent phenyl ring. We note that, for **2**, it is possible that the discontinuity at 290−300 K corresponds to a point of activation of bridge torsional modes.

Conclusions

We have shown that the switch in mechanism from superexchange to thermally activated hopping-dominated transport in the charge recombination of PTZ$^{+\bullet}$-Ph$_n$-PDI$^{-\bullet}$ radical ion pairs, $n > 3$, is induced by activation of the Ph$_n$ torsional motion. This motion allows the bridge to assume a near-coplanar, easily oxidized conformation that may accept a hole from PTZ$^{+\bullet}$. The temperature dependence of charge recombination in the thermally activated region mimics that of the planarization of the bridge. In the temperature regions where superexchange dominates, the temperature dependence of both k_{CR} and the superexchange coupling, V_{DA}, is dictated by a fast conformational equilibrium. This equilibrium increasingly depopulates the reactant state for the CR process as temperature is increased such that CR is negatively activated. However, the electronic coupling, V_{DA}, increases over the same temperature region, leading to the conclusion that CR occurs out of the state with lower effective coupling. A change in vibronic overlap with the product state is suggested as the explanation for overall decline in rate as temperature increases.

Acknowledgment. M.R.W. acknowledges support by the Division of Chemical Sciences, Office of Basic Energy Sciences, U.S. Department of Energy under Grant No. DE-FG02-99ER-14999. M.A.R. acknowledges support from the DARPA MolApps program and the NSF Chemistry Division. E.A.W. would like to thank Dr. Yuri Berlin for many helpful discussions, and Northwestern University and the Link Foundation for fellowships. M.J.T. acknowledges the donors of the American Chemical Society Petroleum Research Fund for partial support of this research.

Supporting Information Available: Experimental details regarding steady-state spectroscopy and the ultrafast transient absorption experiment, a discussion of the semiclassical Marcus description of rate data, as well as additional electrochemical data, calculated reorganization energies, and ion pair energies. This material is available free of charge via the Internet at http://pubs.acs.org.

JA052901J

(89) Mitsui, M. *J. Chem. Phys.* **2002**, *117*, 9740.
(90) Parson, W. W. *Biochim. Biophys. Acta* **1967**, *131*, 154.
(91) Pan, D.; Phillips, D. L. *J. Phys. Chem. A* **1999**, *103*, 4737.